



Epoxy/graphene film for lifecycle self-sensing and multifunctional applications

Sensen Han^{a,b}, Qingshi Meng^{a,b,c,*}, Ke Xing^d, Sherif Araby^d, Yin Yu^a, Adrian Mouritz^e, Jun Ma^{a,d,**}

^a College of Aerospace Engineering, Shenyang Aerospace University, Shenyang, 110136, China

^b Shenyang Aircraft Design Institute, Shenyang, 110001, China

^c State Key Laboratory of Structural Analysis for Industrial Equipment, Dalian University of Technology, Dalian, China

^d University of South Australia, UniSA STEM and Future Industries Institute, SA, 5000, Australia

^e School of Engineering, RMIT University, Melbourne, Victoria, 3001, Australia

ARTICLE INFO

Keywords:

Graphene
Multifunctionality
Self-sensing
Lifecycles

ABSTRACT

Graphene holds promise to provide polymers with multifunctionality such as electrical conductivity. However, pristine graphene is not processable in solvent and graphene oxide even after reduction lacks sufficient electrical conductivity and compatibility with polymers. This work reported an epoxy/graphene nanocomposite film that was synthesized by a facile approach, taking advantage of unique solution-processable graphene platelets (GnPs) that had high structural integrity as reflected by electrical conductivity of 1460 S/cm. A percolation threshold of electrical conductivity was found to be 0.63 vol% for the film. GnPs at 2 vol% improved the thermal conductivity and Young's modulus of epoxy by 117% and 101%, respectively. The film was then investigated as a multifunctional sensor. It can real-time monitor its lifecycle structure health, i.e. the measurement of not only curing parameters but the initiation, localization and evolution of damages spanning from curing to the end of service life. Being sensitive to ambient environmental temperature, the film was investigated as a thermal sensor. Its performance as a strain sensor proved satisfactory through a 20,000-cyclic fatigue test. The film not only self-sensed damage such as cracks but mapped out the corresponding locations. This methodology could lead to the development of cost-effective, high-performance sensors for life-cycle, self-sensing health monitoring for various bonding structures.

1. Introduction

Engineering multifunctionality into polymers has attracted a great deal of interest from both academia and industry over the past decade [1]. Multifunctional materials are usually prepared by combining polymers with specific additives to create new or improved functionalities such as electrical conductivity [2], thermal management [3], barrier property and magnetic and optical performance [4], with mechanical robustness [5]. Also advantageous are multifunctional sensing properties which work in real-time by incorporating sensors such as piezoelectric ceramic transducers or optical fibers into the polymer [6]. However, such sensors often reduce the strength, fracture toughness and other properties of polymers. The limitation is addressed by recently emerged multifunctional [7], self-sensing materials [8], as

outlined below.

Self-sensing refers to the ability of a structural material to sense its own condition, such as strain, stress (which simply relates to strain in an elastic region), damage and temperature. One of the main advantages is that detection is carried out through the whole component volume, i.e. it is not localized as in the case of a typical strain gauge. Self-sensing is attained by exploiting the intrinsic property of structural materials, i.e. the electrical resistivity of carbon fiber nanocomposites as first reported by Baron and Schulte in 1988 [9]. Self-sensing materials are usually based on the incorporation of electrically conductive particles in an insulating polymeric matrix. The particles form an electrical network that can be tuned in accordance with the strain state of the nanocomposite and the presence of discontinuities.

High loading fractions of carbon black (CB) and carbon nanofibers

* Corresponding author. College of Aerospace Engineering, Shenyang Aerospace University, Shenyang, 110136, China.

** Corresponding author. University of South Australia, UniSA STEM and Future Industries Institute, SA, 5000, Australia.

E-mail addresses: mengqingshi@hotmail.com (Q. Meng), Jun.Ma@unisa.edu.au (J. Ma).

(CNFs) have been used in concrete to create self-sensing multifunctional nanocomposites [10,11], although this reduces the mechanical properties. Carbon nanotubes (CNTs) have been added into a polymer compound for structural health monitoring of civil infrastructures [12]. However, it remains a daunting challenge to cost-effectively disentangle these nanotubes in matrices. In comparison with other carbon-based additive materials, graphene has multiple advantages, including exceptionally high electrical conductivity, excellent conformability to substrates, high piezo-sensitivity based on unique contact-breakage mechanisms, and cost-effectiveness when prepared from commercial graphite intercalation compounds [13,14]. Graphene can improve many functional properties of polymers, including increased mechanical properties, enhanced fracture toughness, and superior electrical and thermal conductivities network [15–17].

The two-dimensional structure and very high shape aspect ratio of graphene nanoplatelets (GnPs) make them suitable as reinforcing and conducting fillers in polymers [18–20]. For example, Meng et al. [21] report that adding 0.25 vol% GnPs into epoxy increases the mode I fracture toughness (K_{Ic}) from 0.77 ± 0.07 to 1.82 ± 0.19 MPa $m^{-1/2}$ and the mode I energy release rate G_{Ic} from 0.204 ± 0.03 to 1.01 ± 0.24 kJ m^{-2} . As another example, Zaman et al. [22] found that adding 0.984 vol% unmodified GnPs to an epoxy increases the G_{Ic} by 160%, with a percolation threshold of electrical conductivity recorded at 1.333 vol%.

Graphene is also a promising active material for the development of advanced multi-purpose sensing devices. It has been reported that a graphene-based sensor can detect the pulse rate effectively. Han et al. [23] has developed an epoxy/GnP strain sensor with a gauge factor (GF) of 6, which is much higher than conventional electrical resistance gauges for strain monitoring. Tung et al. [24] developed an epoxy/graphene nanocomposite strain sensor with a GF of 12.8. Additionally, Moriche et al. [25] have reported a 3 wt% epoxy/graphene nanocomposite strain sensor with the GF of ~ 12 at low strain.

Multifunctional self-sensing nanocomposites based on the addition of processable graphene into matrices were developed [15,26–30]. However, it is unknown whether these materials can attain multifunctionality and whether they are applicable to real-time, lifecycle structural health detection. In this work we select epoxy as a representative material to develop multifunctional polymer/graphene nanocomposites having life cycle self-sensing behavior. These mechanically, electrically and thermally enhanced nanocomposites can monitor in real-time not only their own curing process but the initiation and development of damage at micron scale. The real-time detection of the curing parameters – the lowest viscosity point, gelation point and glass transition temperature – provides particularly important information for the design and optimization of manufacturing processes. Through online detection, sudden damage can be readily found and immediately repaired to guarantee structural safety and to enhance the service life. These nanocomposites would be conveniently applied as structural adhesives or coating layers to realize the multifunction.

2. Experiment details

2.1. Material

A graphite intercalation compound (GIC; Asbury 1721; nominal size over 300 μm) was kindly supplied by *Asbury Carbons, Asbury, NJ, USA*. Liquid epoxy resin (E-51, WSR 618) was purchased from *Nantong Xingchen Synthetic Material Co., China*. Epoxy Hardener – Jeffamine D230 (J230) was supplied by *Huntsman, China*.

2.2. Preparation of graphene platelets and their nanocomposites

Graphene platelets (GnPs) were prepared according to a method described by Zaman et al. [31] Briefly, 0.1 g GIC was heat-treated in a furnace at 700 °C for 1 min to induce a thermal shock effect which assisted the subsequent exfoliation. The expanded product was cooled

and then dispersed in acetone using ultrasonication for 2 h below 20 °C (low temperature assisting the exfoliation process) [32].

The GnP-acetone suspension was blended into liquid epoxy resin using magnetic stirring for 20 min followed by ultrasonication for 15 min. During the stirring process the acetone was evaporated by heating the mixture at 80 °C using a hotplate. A vacuum oven at 120 °C was then used to remove bubbles and residual acetone from the liquid epoxy-GnP mixture. The mixture was cooled to 30 °C, and then the hardener J230 was added and manually mixed for 2 min and then cured at 120 °C for 10 h to produce an epoxy/GnP nanocomposite.

Nanocomposites were produced containing different volume fractions of GnPs up to 6 vol%, although most studies were performed on materials with fractions under 2 vol%. An unmodified epoxy without GnPs was prepared as the control material.

2.3. Characterization

The morphology of GnPs and their epoxy nanocomposites was examined by using transmission electron microscopy (TEM) with a Philips CM200 operated at an accelerating voltage of 200 kV. GnPs were suspended in acetone at 0.0004 wt% via 30 min sonication, and a droplet was then deposited onto a 200-mesh lacey copper grids followed by drying. Ultrathin sections (50 nm thick) of the nanocomposites containing different fractions of GnPs were microtomed from bulk samples using a Leica Ultracut S microtome equipped with a diamond knife, and then transferred onto copper grids.

A PerkinElmer 65 FT-IR spectrometer with a Miracle Single Reflection ATR Sample Accessory was used to examine GnPs within the range of 4000–450 cm^{-1} at 2 cm^{-1} increments for a minimum of 32 scans. Raman spectra were recorded by using a Renishaw inVia Raman microspectrometer with 633 nm laser excitation and notch filters cutting set at ~ 100 cm^{-1} .

Tensile testing was performed on dumb-bell shaped samples at an extension loading rate of 0.5 mm/min using a 2 kN load cell tensile machine (XIANGMIN) according to ASTM D-638 specifications. The tensile specimens were 160 mm long, 9.5 mm wide and 5 mm thick, with a gauge length of 25 mm. The Young's modulus was determined over the linear elastic strain range of 0.05–0.15%. Five samples were tested under identical conditions to determine the average value and scatter to the tensile properties. Mode I fracture toughness was measured using CT samples which were 28 mm long (crack growth direction), 36 mm high and 4 mm thick. A pre-crack measuring ~ 12 mm deep was created using a sharp razor blade [33]. At least six tests were repeated for each material at 0.5 mm/min.

The static electrical resistivity of the nanocomposites was measured using an Agilent 4339B high resistivity meter equipped with a 16008B resistivity cell (two-point probe method). The measurements were conducted in accordance with ASTM D257-99 on cylindrical samples that were ~ 5 mm thick and 25 ± 0.5 mm in diameter. The presented data is the average of at least three measurements.

Thermal conductivity of the nanocomposite with a thickness of 0.5 mm and a diameter of 50 mm was measured using a TA Instruments DTC300 analyzer. A sample was placed between two heating plates, and these plates were held at different temperatures (usually 30 °C difference). One of the plates was part of the calibration heat flow meter. An axial temperature gradient was created in the through-thickness direction of the sample, and from this the thermal conductivity was measured.

The curing behavior of a nanocomposite was first examined using dynamic mechanical analysis (DMA) to prepare a benchmark measurement for comparison with those obtained from a Fluke 2638A. A prepreg was made by combining the 1.5 vol% epoxy/GnP mixture with glass fiber by a manual process. A short beam specimen of the prepreg laminate ($36 \times 12 \times 3$ mm) containing GnPs was tested over a temperature range of 25–200 °C at the heating rate of 1 °C/min using a DMA facility (Q800, TA Instrument, USA) operated at the frequency of 1 Hz. Glass

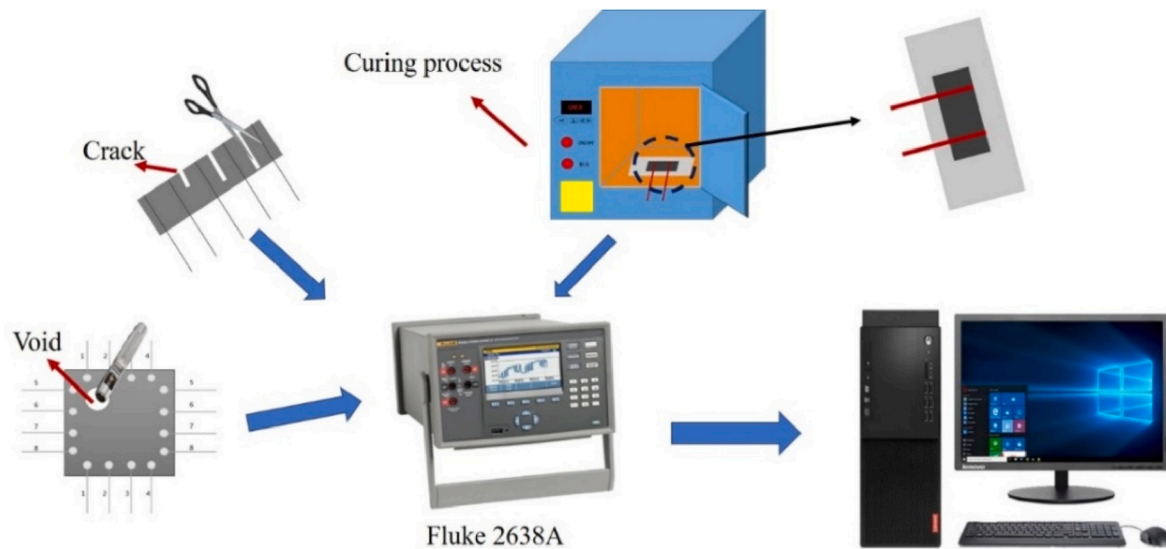


Fig. 1. Schematic of the experimental system.

transition temperatures (T_g) were also measured using DMA at 1 Hz with a single cantilever clamp at a span of 20 mm. The samples were scanned between 25 °C and 120 °C at the heating rate of 5 °C/min.

$$\sigma_c = \sigma_f(\phi - \phi_t)^t \quad (1)$$

where σ_c is the nanocomposite conductivity, σ_f is the proportionality constant, ϕ is the volume fraction of filler ϕ_t is the percolation volume fraction, and t is the critical exponent.

Gauge factors were calculated by

$$GF = \frac{d(\Delta R/R_0)}{d\varepsilon} \quad (2)$$

where ε is the mechanical strain applied to the sensor, and $\Delta R = R - R_0$, where R_0 and R are respectively the resistance of the sensor before and after the deformation.

2.4. Piezo-resistivity evaluation of nanocomposite film

The dynamic electrical resistance of an epoxy/GnP nanocomposite in the form of a thin film was measured with a two-point method using a FLUKE 2638A multimeter, with the monitoring process shown schematically in Fig. 1. The nanocomposite was coated on a glass slide and then cured. The cured film ($30 \times 10 \times 2$ mm) was then carefully removed from the slide, and then tensile tested according to ASTM D638 specification using a loading rate of 0.5 mm/min until failure. Flexural testing of the film was performed according to ASTM D790 at a three-point displacement loading rate of 0.85 mm/min. The flexural test sample dimension was $60 \times 12.7 \times 1.7$ mm, with a support span of 32 mm. Two copper electrical contacts were placed on the film at a spacing of 30 mm using silver paint rings to minimize the electrical contact resistance during tensile and flexural testing.

3. Result and discussion

3.1. Characterization of graphene platelets and their nanocomposite

The morphology of graphene platelets (GnPs) is shown by the transmission electron micrograph presented in Fig. 2a. The thickness of the GnPs was measured to be 2.51 ± 0.39 nm [34], indicating that the platelets consist of 2–4 graphene layers. The nanoplatelets are wrinkled, and enhances the physical interlocking with the epoxy polymer when in a nanocomposite material [35]. A large platelet was selected for electron

diffraction (ED), and the ED pattern reveals the typical six-fold symmetry (Fig. 2b). This further confirms that the GnPs contained a small number of graphene layers.

Fig. 2c shows FT-IR spectrum for the GnPs, and the peaks at 1235 and 870 cm^{-1} indicate the presence of epoxide and ether groups. Fig. 2d presents Raman spectrum for the GnPs, and the peaks at 1340, 1585 and 2715 cm^{-1} correspond respectively to the D-, G- and 2D-bands. The D-band intensity usually increases with the degree of oxidation and impurity content whereas the high G-band intensity indicates a regular graphitic structure [36]. The measured D- to G-band ratio of 0.07 is much smaller than that of graphite oxide [37,38], indicating that the GnPs have a low oxidation degree and relatively few defects.

The exfoliation and dispersion of GnPs in polymers are two critical factors determining the mechanical, electrical, thermal and other functional properties of nanocomposites. Fig. 2(e)–(f) present TEM micrographs showing the typical dispersion of GnPs (1.5 vol%) within an epoxy nanocomposite. The GnPs show no significant agglomeration or clustering, with the nanoplatelets being relatively uniformly dispersed in epoxy matrix phase.

3.2. Nanocomposite properties

The electrical conductivity of the epoxy polymer increases by orders of magnitude upon compounding with increasing volume fractions of the GnPs, as shown in Fig. 3a. By fitting the experimental data into Eq. (1), the percolation threshold (i.e. the formation of pathways for electron transfer) was calculated to be 0.63 vol%, as shown in the bottom right corner of Fig. 3a. The formation of an electrically conductive network at such a low threshold leads to the following conclusions: i) GnPs each should be sufficiently thin to counter the side effect of their poor through-plane conductivity, ii) GnPs must be uniformly dispersed in the epoxy matrix and iii) most of GnPs are in close physical contact. *Noteworthy is that different equations were adopted for the calculation of the electrical conductivity threshold for polymer/carbon nanotube nanocomposites [39,40].*

The thermal conductivity of the epoxy rises gradually with increasing GnP content up to ~2 vol%, as shown in Fig. 3b, but at higher contents the conductivity rises more rapidly. At relatively low GnP contents the platelets are spaced sufficiently far apart that there is high Kapitza resistance (i.e. thermal boundary resistance) and hence overall low thermal conductivity. With increasing GnP content up to 6 vol%, the interdistance between the platelets becomes shorter leading to an increased likelihood of contact which is needed for effective phonon

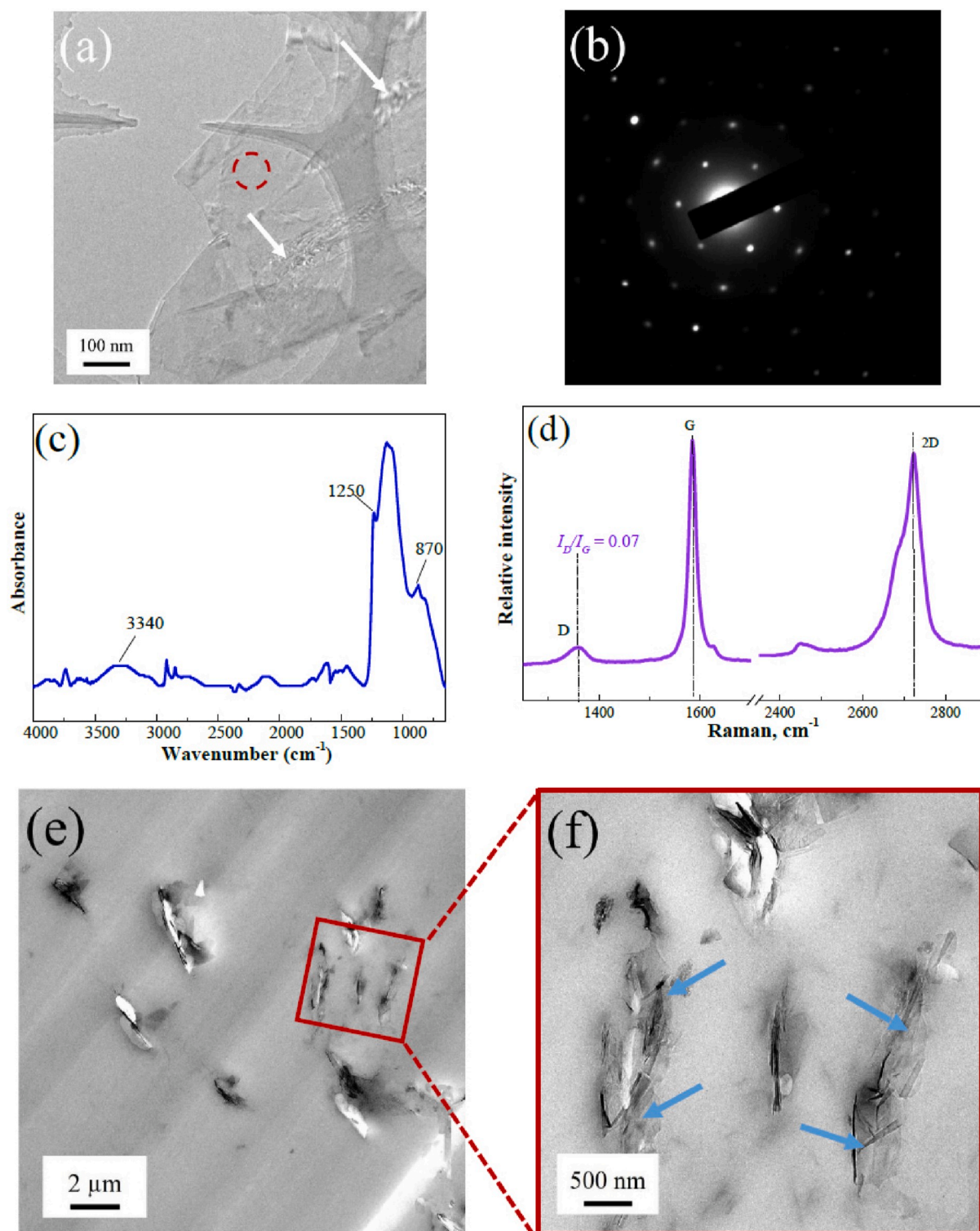


Fig. 2. (a) TEM micrograph, (b) electron diffraction pattern, (c) FT-IR spectrum and (d) Raman spectrum of GnPs; (e) and (f) TEM micrographs of an epoxy/GnP nanocomposite at 1.5 vol%.

transfer via lattice vibration. In this study, the thermal conductivity reaches $2.17 \text{ W m}^{-1} \text{ K}^{-1}$ at 6 vol%, which is a 13-fold increase over the neat epoxy. The improvement is attributed to the high thermal conductivity of thin GnPs.

The effect of increasing GnP content of the tensile properties of the nanocomposites is shown in Fig. 3c. The modulus increases with GnP fraction reaching a maximum of 3.17 GPa, which is twice as high as the neat epoxy. However, the tensile failure stress decreases with increasing

GnP content. For epoxy having relatively low modulus, tensile strength may increase by introducing inorganic nanosheets [22,41]. However, these nanosheets often reduce the tensile strength of brittle epoxy resins and PMMA [42–44]. The tensile strength is often reduced due to agglomeration of the nanoparticles, which act as a geometric stress raiser in the polymer matrix and thereby lower the stress needed to initiate cracking which caused tensile failure. This explains the obvious drop in tensile strength in Fig. 3c. Nevertheless, these films would be

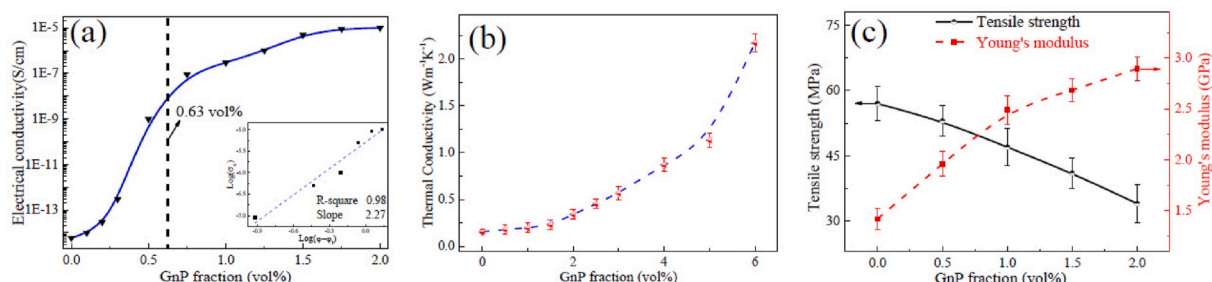


Fig. 3. The electrical, thermal and mechanical properties of epoxy/GnP nanocomposites.

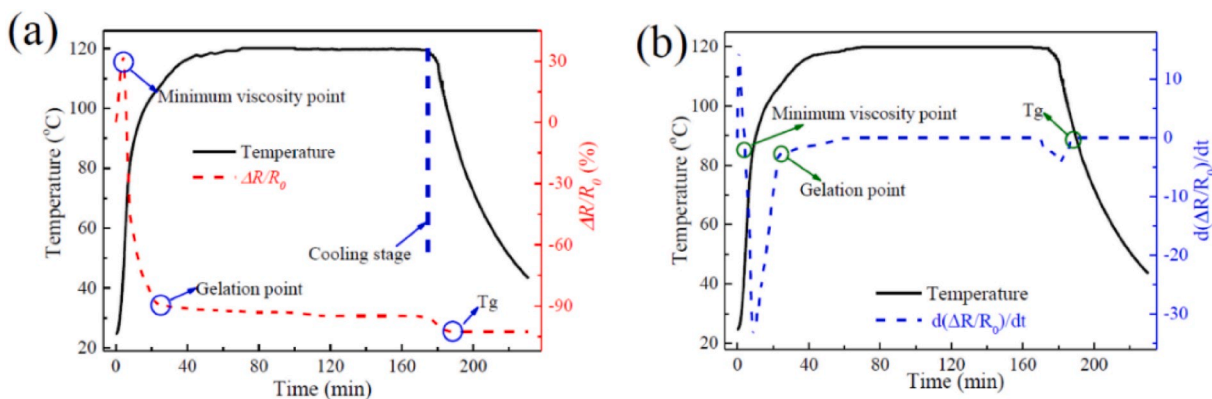


Fig. 4. Relative resistance of 1.5 vol% nanocomposite during curing: (a) resistance change graphs vs temperature and (b) their differential graphs.

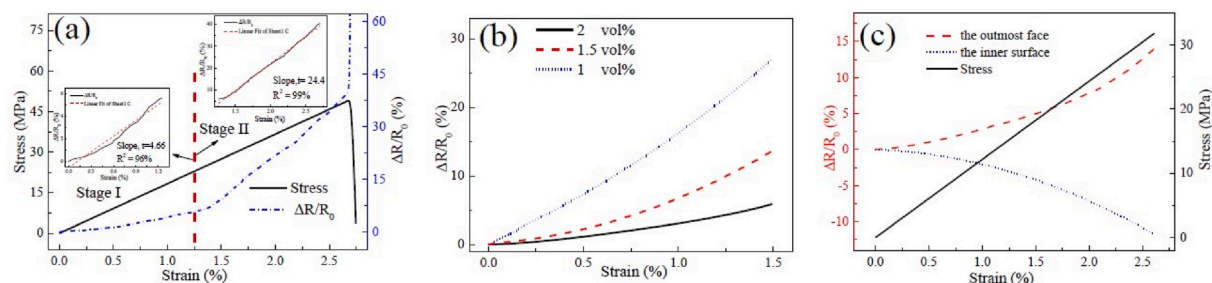


Fig. 5. Electrical response of (a) 1.5 vol% nanocomposite film under tensile loading, (b) effect of GnP content on the resistance change under tensile loading and (c) 1.5 vol% nanocomposite film under flexural loading.

sufficiently strong and deformable for applications such as self-sensing strain sensors.

3.3. Lifecycle self-monitoring using the nanocomposite films

3.3.1. Curing process monitoring

Critical manufacturing parameters for epoxy nanocomposites are often determined by monitoring its curing behavior, which would enable the manufacturers to scale up a technology. The curing process used in this study consists of three main stages: (1) heating from room temperature to 120 °C, (2) isothermal heating at 120 °C for 2 h, and (3) cool-down from 120 °C to room temperature. Since our nanocomposites are electrically conductive, the curing characteristic of these three stages can be monitored in real-time via changes to the electrical resistance, as shown in Fig. 4. Initially, the relative resistance change $\Delta R/R_0$ increases to 33% at 47 °C (see Fig. 4a), and then it drops sharply by $\sim 123\%$ down to -90% when the temperature reaches 105 °C. In the subsequent isothermal cure stage (stage 2), the $\Delta R/R_0$ value gradually approaches a constant resistance change value of -95% . During cool-down (stage 3), $\Delta R/R_0$ decreases linearly from -95% to -103% , and then reaches a

constant value at room temperature when in the fully cured condition. The resistance change reflects the physical state changes of the epoxy matrix in the curing process. As curing proceeds, the cross-linking density of the epoxy increases rapidly as well as the matrix shrinks. These processes push the platelets closer together and thereby reduce the electrical resistance and causing the $\Delta R/R_0$ to reach a negative value (Fig. 4a). Detailed analysis is revealed in the Supporting Information Section 1.1. Although $\Delta R/R_0$ is appropriate for data interpretation, $d(\Delta R/R_0)/dt$ is used herein to show more clearly the inflection point in $\Delta R/R_0$, and it can identify the lowest viscosity, gelation point, and T_g during the curing process (Fig. 4b).

By tracking the resistance change during a dynamic heating process, we found the lowest viscosity, gelation point and T_g were measured to be 47, 105 and 96 °C, respectively (Fig. 4a & b); these values are very close to those measured using DMA, i.e. 49, 108 and 98 °C, which is reported in the Supporting Information Section 1.2.

3.3.2. Real-time, lifecycle strain sensing

A nanocomposite at 1.5 vol% GnPs was selected to study piezoelectric sensing performance, since the GnP loading is slightly over the

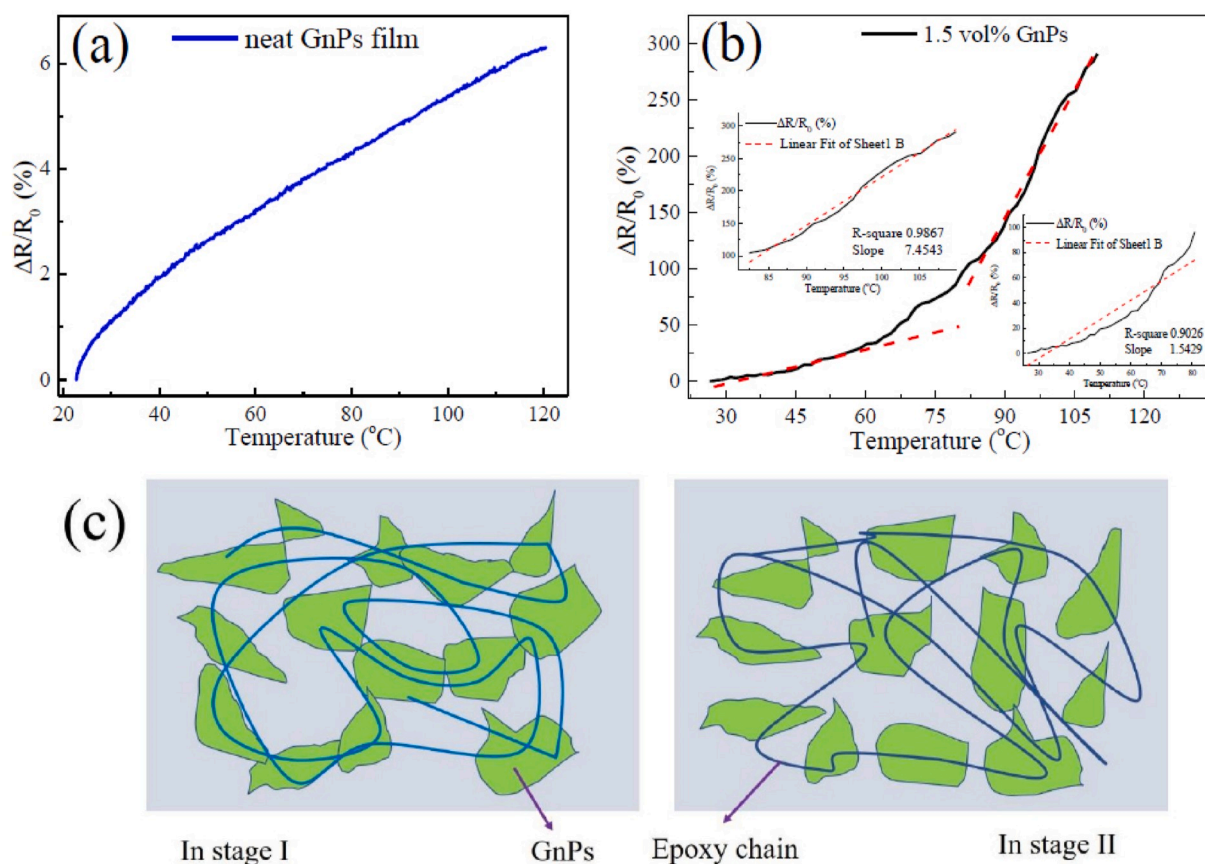


Fig. 6. Electrical response during dynamic heating: (a) neat GnP film and (b) epoxy/GnP nanocomposite at 1.5 vol% and (c) schematic change of GnP's.

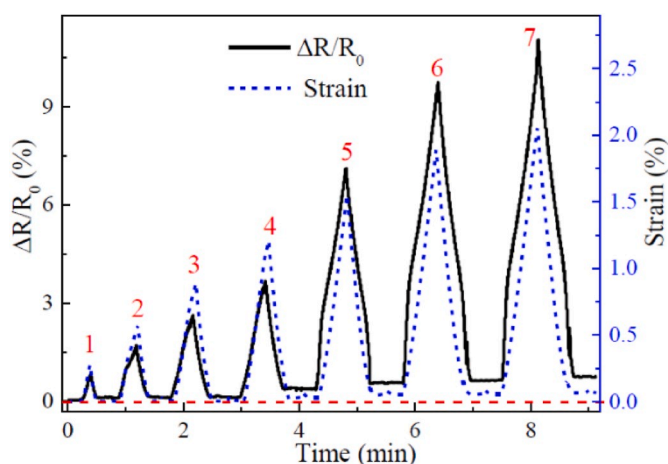


Fig. 7. Cyclic loading with transient strain and resistance response.

percolation threshold; GnP's in the nanocomposite are anticipated to connect with each other by tunneling or/and overlapping to achieve sensing performance with stability. Fig. 5a and b shows the piezoresistive behavior under quasi-static tensile loading. Fig. 5a illustrates schematically two general stages of damage progression in the nanocomposite film, where the electrical resistance increases until fracture due to the breakage of conductive networks. In stage I where strain $< 1.25\%$, the increase of resistance tends to be linear, and in stage II where strain $> 1.25\%$, the resistance change presents a different linear growth. These two stages have sensitivity (GF, Eq. (2)) of 4.66 and 24.4. At a low strain level of 0–1.25%, the application of external tension

results in a low expansion of tunneling pathways so the tunneling resistance increases, while at a strain range of 1.25%–2.70%, it is possibly associated with disconnection or separation between adjacent GnP's during the test. The electrical resistance change is more pronounced at higher strain rates, showing a clear exponential behavior. Hence, a prevalence of out of plane contact mechanisms is found at lower strain levels whereas a prevalence of in-plane transport mechanisms is found at higher strain levels [45].

The sensitivity of the nanocomposite films to the applied tensile stress was dependent on the GnP content, as shown in Fig. 5b, with sensitivity values at low strain of 18 ± 2.1 , 9.2 ± 1.4 and 3.9 ± 0.8 for the nanocomposites containing GnP's of 1.0, 1.5 and 2.0 vol%, respectively. It is noteworthy that sensitivity values were calculated with a constant strain interval in all cases to facilitate comparison.

The nanocomposite films were also capable of detecting stress under flexural loading, as shown in Fig. 5c. However, due to the upper and lower surfaces of the specimen experiencing compression and tension strains respectively, the resistivity changes in these surfaces were also different. For one surface subject to compression, stress linearly increases to 32 MPa with strain, and $\Delta R/R_0$ decreases from 0 to -12%. For the other surface subject to tension, stress increases to 32 MPa and $\Delta R/R_0$ to 14% (Fig. 5c). Since the inter-nanosheet resistance of GnP's in epoxy is controlled by modulation of charge-hopping transport and carrier mobility by coupling at nanosheet junctions [46,47], the graphene network is expected to change greatly upon straining. Tensile strain may reduce coupling at nanosheet junctions, leading to an increase to the resistance whereas the compressive strain may induce coupling at nanosheet junctions leading to a reduction to the resistance.

3.3.3. Temperature sensing

Temperature monitoring using smart sensors is useful for a diverse

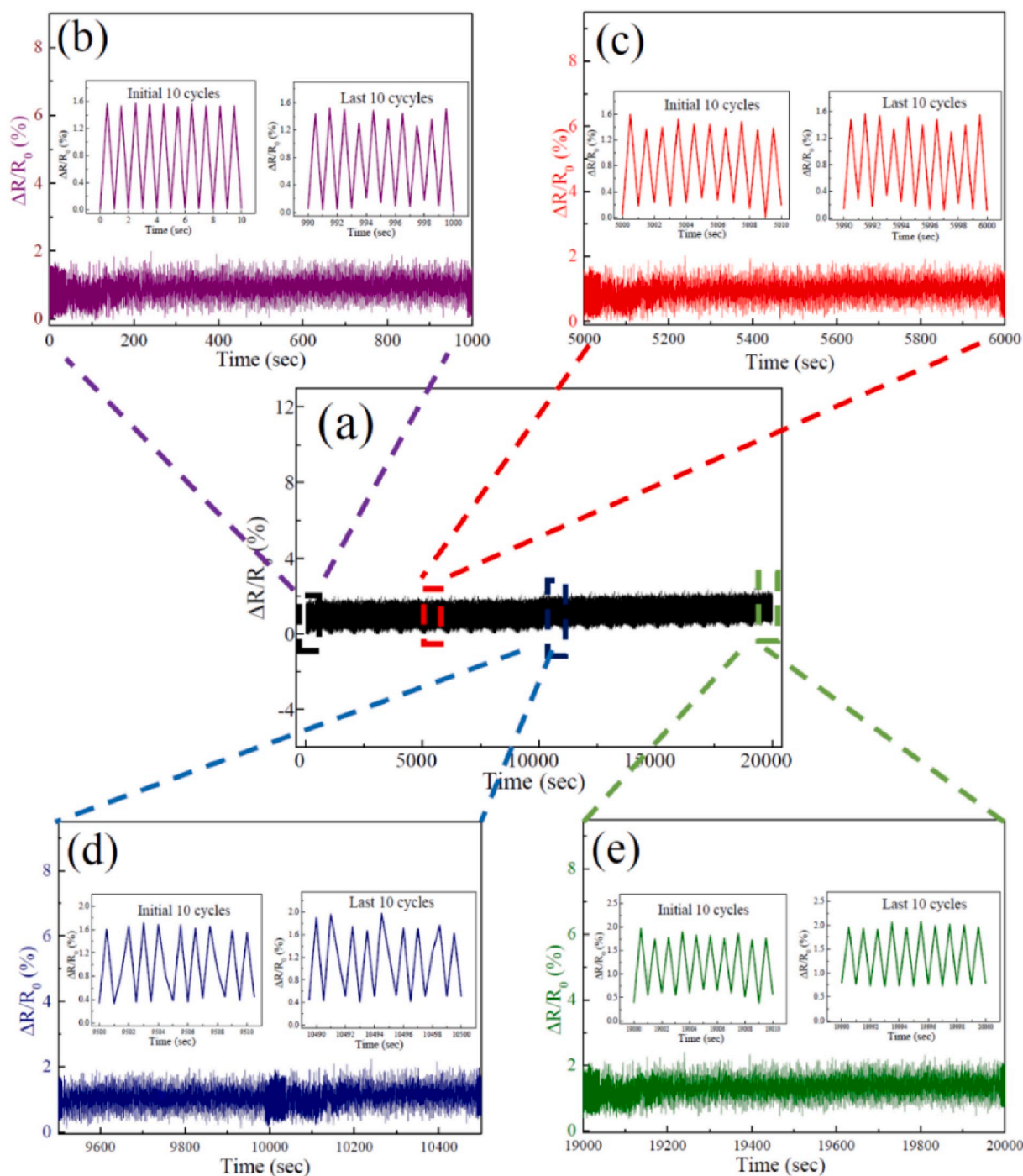


Fig. 8. Resistance change ($\Delta R/R_0$) up to 20,000 cycles for strains at a frequency of 1 cycle/sec.

range of applications using electronic, chemical, mechanical and biological systems [48]. It was found that the electrical resistance of the neat GnP film increases with temperature, as shown in Fig. 6a. In comparison, the bulk GnP nanocomposite is much more sensitive to temperature changes, as shown by the normalized electrical resistance curve in Fig. 6b, with $\Delta R/R_0$ increasing by nearly 300% when the temperature is increased from 25 °C to 110 °C. Over this temperature range, the $\Delta R/R_0$ –temperature curve for the bulk nanocomposite can be divided into two stages. In stage I (25–60 °C) the $\Delta R/R_0$ curve increases at a relatively slow rate, and this is due to the relatively low mobility of the epoxy molecules (Fig. 6c).

In stage II (above ~60 °C), the epoxy molecules experience increased rotational and translational motions with increasing temperature

causing movement and separation of GnPs (Fig. 6c) resulting in increased electrical resistance. In general, for a polymer heated from a solid state, its glass transition temperature may be defined as the temperature at which molecular rotation about single bonds becomes unconstrained. There is a sufficient increase in thermal energy in stage II to allow movement of relatively large molecular segments of the epoxy, which can rotate about carbon-carbon single bonds when the resin is heated [49]. In the glass transition region, the heat flow to the sample increases as the polymer absorbs the thermal energy necessary for molecular rotation. The heat capacity increases discontinuously as the resin changes from a glass to a more fluid rubbery material. The $\Delta R/R_0$ curve increases most rapidly above ~90 °C when the bulk nanocomposite becomes rubbery.

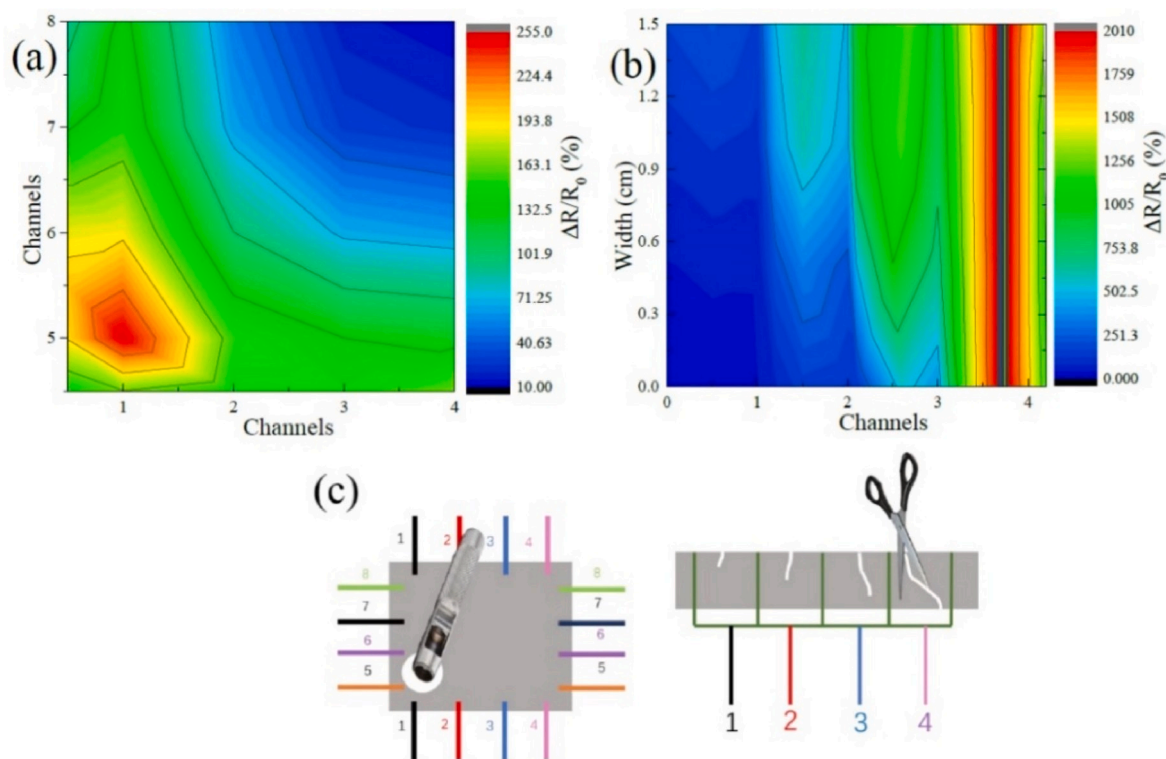


Fig. 9. Electrical response of 1.5 vol% nanocomposite film for self-sensing damage: (a) self-damage localization and (b) crack length evaluation.

3.3.4. Loading-unloading cycles and fatigue performance

In order to track damage accumulation in a nanocomposite using changes to the electrical resistivity, specimens were subjected to cyclic tensile loading with a progressively increasing step load. The effect of increasing number of load cycles on the normalized electrical resistivity and the strain of the nanocomposite film is shown in Fig. 7, and there is a correlation. The amplitude of $\Delta R/R_0$ increases with the tensile strain experienced by the nanocomposite film. In the first four cycles where strain is below 1.25%, the increase to the electrical resistance closely followed the increase to the strain; and upon unloading both the resistance and strain returned to their original values, which demonstrates good coupling between the electrical and mechanical responses. This agrees with the elastic deformation response of the bulk nanocomposite under tensile loading up to strain of $\sim 1.25\%$ (Fig. 5a). When the nanocomposite film was subjected to higher strain values (i.e. 5-7th load cycles), which exceeded the elastic limit, then the electrical resistance did not fully return to the original value upon unloading, and this is attributed to the formation of micro-cracks at the GnP-epoxy interfaces within the film [50–52].

The nanocomposite film was also subjected to 20,000 cycles of tensile loading-unloading over the strain range of 0–0.25% at the frequency of 1 Hz to evaluate the long-term sensing durability. Under these conditions, there was no measurement change to the maximum $\Delta R/R_0$ value over the 20,000 cycles, as shown in Fig. 8a. Fig. 8b shows electrical resistivity of the film over the initial 1000 cycles, and the resistivity changes are immediate upon the application of cyclic loads. When the $\Delta R/R_0$ values within the first 10 load cycles are compared with the values within the last 10 cycles in Fig. 8b inset, the film still responds immediately to the strain. Fig. 8c shows the sensing performance for 5000–6000 cyclic loading, and in Fig. 8c insets $\Delta R/R_0$ within the first 10 s were compared to those within the last 10 s. It shows no obvious deterioration to the sensing performance of the film. Fig. 8d shows the performance for 9500–10,500 cyclic loading, where a very minor degeneration phenomenon is observed. Upon loading-unloading, $\Delta R/R_0$ decreases from 1.8% to 0.6% in comparison with the 1.5%–0.4% in the

first 10 cycles in Fig. 8d, suggesting damage occurred in the nanocomposite film sensor. The continuous loading-unloading cycles have gradually changed the morphology/layout of GnPs as well as the distance between them, resulting in an evolution of conductive networks in the film. Fig. 8e shows the sensing performance for 19,000–20,000 cyclic loading. The magnified insets show a similar minor degeneration to Fig. 8e; with $\Delta R/R_0$ decreasing to 0.75% upon unloading. This phenomenon might relate to the irreversible destruction of the conductive networks as well as the disruption of epoxy chains.

As analyzed above, the nanocomposite film sensor can respond relatively stable at a micro-strain level during a long period of cyclic loading. With over 10,000 cyclic loading, there is only a minor increment of the max $\Delta R/R_0$, suggesting a very low degree of irreversible damage to the nanocomposite film sensor.

3.3.5. Damage localization and crack evolution

The detection and localization of damage in structural components are important for effective maintenance and repair. The capacity of the nanocomposite film to detect the location of damage using changes to electrical resistivity was evaluated for a drilled hole. An array of narrow strips on the film ($60 \times 60 \times 2$ mm) were applied to connect the data collector (Fluke), as shown schematically in Fig. 9a. These channels were selected to identify the damage location by comparing the electrical resistivity measurements from the different films. Immediately after drilling (Fig. 9c), a significant resistance change was measured for all channels. The $\Delta R/R_0$ values for channels 1 and 5 had the largest increases; 1241% and 918% respectively. Channels 2 and 6 had lower resistivity increases of 396% and 423%, respectively, whereas channels 3, 4, 7 and 8 had the lowest increases (between 35% and 136%). By comparing the resistivity values measured by the different film strips, the drilled hole was accurately detected in the bottom left region, being close to channels 1, 2, 5 and 6, in agreement with the actual location.

The monitoring of crack propagation in structural components is an important structural health monitoring functionality. To monitor crack growth, four nanocomposite films were fitted with four channels

(Fig. 9c), through which the electrical response was measured as indicated in Fig. 9b. During the measurement, scissors were used to cut into the films to create three cracks of 3, 6 and 9 cm in length, to separate the film into halves. Upon cutting, the $\Delta R/R_0$ of channel 1, 2 and 3 abruptly increased from initial values 0%–209%, 439% and 1034%, respectively. Subsequently, the resistance of channel 4 suddenly increases until the resistance reading disappears. By comparing the resistance change, it concludes that the crack length follows channel 3 > channel 2 > channel 1, with the channel 4 showing infinite resistance change.

4. Conclusion

In summary, we developed an epoxy/graphene nanocomposite film which demonstrated sufficient mechanical, electrical and thermal properties for lifecycle self-sensing. The film can sense its own curing process by monitoring the parameters of viscosity, gelation point and glass transition temperature; such a function is critical to quality assurance in manufacturing multifunctional nanocomposites. The nanocomposite film proved valuable in sensing temperature, damage detection and mapping, and mechanical loading and unloading of 20,000 cycles. The multifunctional self-sensing nanocomposite film would have considerable potential applications in various bonding structures for safety condition monitoring. Furthermore, the nanocomposite is capable to work as a smart adhesive for monitoring of bonded joints in structures. Graphene at 0.5 vol% improved the lap shear strength from 11.37 ± 0.30 to 14.13 ± 0.28 MPa, and it at 1.5 vol% enhanced adhesive toughness from 48 ± 15 to 265 ± 20 J/m², an increment of 463%. Overall, graphene significantly improved the mechanical, electrical and thermal properties of epoxy, enabling the nanocomposite film to be used as a multifunctional sensor.

Declaration of competing interest

The authors declare that they have no known competing financial interests or personal relationships that could have appeared to influence the work reported in this paper.

CRediT authorship contribution statement

Sensen Han: Writing - original draft. **Qingshi Meng:** Conceptualization, Methodology, Resources, Supervision, Funding acquisition. **Ke Xing:** Visualization, Investigation. **Sherif Araby:** Visualization, Supervision. **Yin Yu:** Validation. **Adrian Mouritz:** Writing - review & editing. **Jun Ma:** Writing - review & editing, Supervision.

Acknowledgement

QM and JM thank Asbury (*Asbury, NJ, USA*) for providing the GIC (1721). This work was financially supported by the the Natural Science Foundation of Liaoning Province (2019-MS-256), Aeronautical Science Foundation of China (2018ZF54036), China Postdoctoral Science Foundation (2019M651151), National Natural Science Foundation of China (51973123) and the plan of rejuvenating the talents of Liaoning province (XLYC1907135). JM thanks financial support by the Australian Research Council (DP200101737).

Appendix A. Supplementary data

Supplementary data to this article can be found online at <https://doi.org/10.1016/j.compscitech.2020.108312>.

References

- [1] H. Bai, C. Li, G. Shi, Functional composite materials based on chemically converted graphene, *Adv. Mater.* 23 (9) (2011) 1089–1115.

- [2] S. Stankovich, D.A. Dikin, G.H. Dommett, K.M. Kohlhaas, E.J. Zimney, E.A. Stach, R.D. Piner, S.T. Nguyen, R.S. Ruoff, Graphene-based composite materials, *Nature* 442 (7100) (2006) 282.
- [3] S. Araby, Q. Meng, L. Zhang, I. Zaman, P. Majewski, J. Ma, Elastomeric composites based on carbon nanomaterials, *Nanotechnology* 26 (11) (2015) 112001.
- [4] W. Wu, R. Tang, Q. Li, Z. Li, Functional hyperbranched polymers with advanced optical, electrical and magnetic properties, *Chem. Soc. Rev.* 44 (12) (2015) 3997–4022.
- [5] Q. Meng, C.H. Wang, S. Nasser, H.-C. Kuan, J. Dai, K. Friedrich, J. Ma, Nanosilica-toughened polymer adhesives, *Mater. Des.* 61 (2014) 75–86.
- [6] K. Michel, B. Bureau, C. Boussard-Plédel, T. Jouan, J. Adam, K. Staubmann, T. Baumann, Monitoring of pollutant in waste water by infrared spectroscopy using chalcogenide glass optical fibers, *Sensor. Actuator. B Chem.* 101 (1-2) (2004) 252–259.
- [7] X. Shen, Z. Wang, Y. Wu, X. Liu, J.-K. Kim, Effect of functionalization on thermal conductivities of graphene/epoxy composites, *Carbon* 108 (2016) 412–422.
- [8] D.D.L. Chung, Carbon materials for structural self-sensing, electromagnetic shielding and thermal interfacing, *Carbon* 50 (9) (2012) 3342–3353.
- [9] D. Chung, Self-sensing Structural Composites in Aerospace Engineering, *Advanced Composite Materials for Aerospace Engineering*, Elsevier, 2016, pp. 295–331.
- [10] H. Li, H.-g. Xiao, J.-p. Ou, Effect of compressive strain on electrical resistivity of carbon black-filled cement-based composites, *Cement Concr. Compos.* 28 (9) (2006) 824–828.
- [11] B. Han, S. Ding, X. Yu, Intrinsic self-sensing concrete and structures: a review, *Measurement* 59 (2015) 110–128.
- [12] J.L. Abot, Y. Song, M.S. Vatsavaya, S. Medikonda, Z. Kier, C. Jayasinghe, N. Rooy, V.N. Shanov, M.J. Schulz, Delamination detection with carbon nanotube thread in self-sensing composite materials, *Compos. Sci. Technol.* 70 (7) (2010) 1113–1119.
- [13] L.M. Chiacchiarelli, M. Rallini, M. Monti, D. Puglia, J.M. Kenny, L. Torre, The role of irreversible and reversible phenomena in the piezoresistive behavior of graphene epoxy nanocomposites applied to structural health monitoring, *Compos. Sci. Technol.* 80 (2013) 73–79.
- [14] W.C. Tan, W.H. Shih, Y.F. Chen, A highly sensitive graphene-organic hybrid photodetector with a piezoelectric substrate, *Adv. Funct. Mater.* 24 (43) (2015) 6818–6825.
- [15] M.S. Rocio Moriche, Silvia G. Prolongo, Alberto Jiménez-Suárez, Alejandro Ureña, Reversible phenomena and failure localization in self-monitoring GNP/epoxy nanocomposites, *Compos. Struct.* (136) (2016) 101–105.
- [16] S. Wang, D. Chung, Self-sensing of flexural strain and damage in carbon fiber polymer-matrix composite by electrical resistance measurement, *Carbon* 44 (13) (2006) 2739–2751.
- [17] R. Balaji, M. Sasikumar, Graphene based strain and damage prediction system for polymer composites, *Compos. Appl. Sci. Manuf.* 103 (2017) 48–59.
- [18] S. Han, Q. Meng, Z. Qiu, A. Osman, R. Cai, Y. Yu, T. Liu, S. Araby, Mechanical, toughness and thermal properties of 2D material-reinforced epoxy composites, *Polymer* 184 (2019).
- [19] Q. Meng, S. Han, S. Araby, Y. Zhao, Z. Liu, S. Lu, Mechanically robust, electrically and thermally conductive graphene-based epoxy adhesives, *J. Adhes. Sci. Technol.* (2019) 1–20.
- [20] S. Han, Q. Meng, A. Chand, S. Wang, X. Li, H. Kang, T. Liu, A comparative study of two graphene based elastomeric composite sensors, *Polym. Test.* 80 (2019).
- [21] Q. Meng, J. Jin, R. Wang, H.C. Kuan, J. Ma, N. Kawashima, A. Michelmoro, S. Zhu, C.H. Wang, Processable 3-nm thick graphene platelets of high electrical conductivity and their epoxy composites, *Nanotechnology* 25 (12) (2014) 125707.
- [22] I.K. Zaman, H.C. Dai, J. Kawashima, N. Michelmoro, A. Sovi, A. Dong, S. Luong, L. J. Ma, From carbon nanotubes and silicate layers to graphene platelets for polymer nanocomposites, *Nanoscale* 4 (15) (2012) 4578–4586.
- [23] S. Han, A. Chand, S. Araby, R. Cai, S. Chen, H. Kang, R. Cheng, Q. Meng, Thermally and electrically conductive multifunctional sensor based on epoxy/graphene composite, *Nanotechnology* 31 (7) (2019), 075702.
- [24] T.T. Tung, R. Karunakaran, D.N.H. Tran, B. Gao, S. Nag-Chowdhury, I. Pillin, M. Castro, J.-F. Feller, D. Losic, Engineering of graphene/epoxy nanocomposites with improved distribution of graphene nanosheets for advanced piezo-resistive mechanical sensing, *J. Mater. Chem. C* 4 (16) (2016) 3422–3430.
- [25] R. Moriche, M. Sánchez, A. Jiménez-Suárez, S.G. Prolongo, A. Ureña, Strain monitoring mechanisms of sensors based on the addition of graphene nanoplatelets into an epoxy matrix, *Compos. Sci. Technol.* 123 (2016) 65–70.
- [26] S. Dai Pang, H.J. Gao, C. Xu, S.T. Quek, H. Du, Strain and damage self-sensing cement composites with conductive graphene nanoplatelet, sensors and smart structures technologies for civil, mechanical, and aerospace systems 2014, *Int. Soc. Opt. Photon.* (2014) 906126.
- [27] Q. Meng, V. Kenelak, A. Chand, H. Kang, S. Han, T. Liu, A Highly Flexible, Electrically Conductive, and Mechanically Robust Graphene/epoxy Composite Film for its Self-Damage Detection, 2020.
- [28] Q. Meng, Z. Liu, R. Cai, S. Han, S. Lu, T. Liu, Non-oxidized graphene/elastomer composite films for wearable strain and pressure sensors with ultra-high flexibility and sensitivity, *Polym. Adv. Technol.* 31 (2) (2019) 214–225.
- [29] Q. Meng, Y. Zhao, Z. Liu, S. Han, S. Lu, T. Liu, Flexible strain sensors based on epoxy/graphene composite film with long molecular weight curing agents, *J. Appl. Polym. Sci.* 136 (35) (2019) 47906.
- [30] Q. Meng, Z. Liu, S. Han, L. Xu, S. Araby, R. Cai, Y. Zhao, S. Lu, T. Liu, A facile approach to fabricate highly sensitive, flexible strain sensor based on elastomeric/graphene platelet composite film, *J. Mater. Sci.* 54 (2019) 10856–10870.
- [31] I.K. Zaman, Hsu-Chiang Meng, Qingshi Michelmoro, Andrew Kawashima, Nobuyuki Pitt, Terry Zhang, Liqun Gouda, Sherif Luong, Ma Lee, Jun, A facile

- approach to chemically modified graphene and its polymer nanocomposites, *Adv. Funct. Mater.* 22 (13) (2012) 2735–2743.
- [32] I. Zaman, H.C. Kuan, J. Dai, N. Kawashima, A. Michelmore, A. Sovi, S. Dong, L. Luong, J. Ma, From carbon nanotubes and silicate layers to graphene platelets for polymer nanocomposites, *Nanoscale* 4 (15) (2012) 4578–4586.
- [33] Q.Z. Meng, Izzuddin, J.R. Hannam, S. Kapota, L. Luong, O. Youssf, J. Ma, Improvement of adhesive toughness measurement, *Polym. Test.* 30 (2) (2011) 243–250.
- [34] I. Zaman, H.-C. Kuan, Q. Meng, A. Michelmore, N. Kawashima, T. Pitt, L. Zhang, S. Gouda, L. Luong, J. Ma, A facile approach to chemically modified graphene and its polymer nanocomposites, *Adv. Funct. Mater.* 22 (13) (2012) 2735–2743.
- [35] I. Srivastava, R.J. Mehta, Z.Z. Yu, L. Schadler, Raman study of interfacial load transfer in graphene nanocomposites, *Appl. Phys. Lett.* 98 (6) (2011) 282.
- [36] J.M. Ma, Qingshi Zaman, Izzuddin Zhu, Shenmin Michelmore, Andrew Kawashima, Nobuyuki Wang, Chun H. Kuan, Hsu-Chiang, Development of polymer composites using modified, high-structural integrity graphene platelets, *Compos. Sci. Technol.* 91 (2014) 82–90.
- [37] M.C. Hsiao, S.H. Liao, M.Y. Yen, P. Liu, N.W. Pu, C.A. Wang, C.C.M. Ma, Preparation of covalently functionalized graphene using residual oxygen-containing functional groups, *ACS Appl. Mater. Interfaces* 2 (11) (2010) 3092.
- [38] G. Wang, X. Shen, B. Wang, J. Yao, Jinsoo Park, Synthesis and characterisation of hydrophilic and organophilic graphene nanosheets, *Carbon* 47 (5) (2009) 1359–1364.
- [39] N. Hu, Z. Masuda, H. Fukunaga, Prediction of electrical conductivity of polymer filled by carbon nanotubes, in: *Proceedings of the 16th International Conference on Composite Materials*, 2007.
- [40] X.F. Sánchez-Romate, A. Jiménez-Suárez, M. Sánchez, A. Güemes, A. Ureña, Novel approach to percolation threshold on electrical conductivity of carbon nanotube reinforced nanocomposites, *RSC Adv.* 6 (49) (2016) 43418–43428.
- [41] J. Ma, Q. Meng, A. Michelmore, N. Kawashima, Z. Izzuddin, C. Bengtsson, H.-C. Kuan, Covalently bonded interfaces for polymer/graphene composites, *J. Mater. Chem. A* 1 (13) (2013) 4255.
- [42] I. Zaman, B. Manshoor, A. Khalid, Q. Meng, S. Araby, Interface modification of clay and graphene platelets reinforced epoxy nanocomposites: a comparative study, *J. Mater. Sci.* 49 (17) (2014) 5856–5865.
- [43] Q. Meng, H.C. Kuan, S. Araby, N. Kawashima, N. Saber, C.H. Wang, J. Ma, Effect of interface modification on PMMA/graphene nanocomposites, *J. Mater. Sci.* 49 (17) (2014) 5838–5849.
- [44] S. Han, Q. Meng, X. Pan, T. Liu, S. Zhang, Y. Wang, S. Haridy, S. Araby, Synergistic effect of graphene and carbon nanotube on lap shear strength and electrical conductivity of epoxy adhesives, *J. Appl. Polym. Sci.* 136 (42) (2019) 48991.
- [45] M. Sánchez, R. Moriche, X.F. Sánchez-Romate, S. Prolongo, J. Rams, A. Ureña, Effect of graphene nanoplatelets thickness on strain sensitivity of nanocomposites: a deeper theoretical to experimental analysis, *Compos. Sci. Technol.* 181 (2019) 107697.
- [46] G. Eda, M. Chhowalla, Graphene-based composite thin films for electronics, *Nano Lett.* 9 (2) (2009) 814–818.
- [47] T.Q. Trung, N.T. Tien, D. Kim, J.H. Jung, O.J. Yoon, N.-E. Lee, High thermal responsiveness of a reduced graphene oxide field-effect transistor, *Adv. Mater.* 24 (38) (2012) 5254–5260.
- [48] M. Mohiuddin, K.K. Sadasivuni, S. Mun, J. Kim, Flexible cellulose acetate/graphene blueprints for vibrotactile actuator, *RSC Adv.* 5 (43) (2015) 34432–34438.
- [49] A. Lerf, A. Buchsteiner, J. Pieper, S. Schöttl, I. Dekany, T. Szabo, H. Boehm, Hydration behavior and dynamics of water molecules in graphite oxide, *J. Phys. Chem. Solid.* 67 (5-6) (2006) 1106–1110.
- [50] J. Zhang, J. Liu, R. Zhuang, E. Mäder, G. Heinrich, S. Gao, Single MWNT-glass fiber as strain sensor and switch, *Adv. Mater.* 23 (30) (2011) 3392–3397.
- [51] E.T. Thostenson, T.W. Chou, Real-time in situ sensing of damage evolution in advanced fiber composites using carbon nanotube networks, *Nanotechnology* 19 (21) (2008) 215713.
- [52] G. Pandey, M. Wolters, E.T. Thostenson, D. Heider, Localized functionally modified glass fibers with carbon nanotube networks for crack sensing in composites using time domain reflectometry, *Carbon* 50 (10) (2012) 3816–3825.